Collapse Behavior of Pultruded FRP Shapes and the Structural Health Monitoring

Seishi YAMADA*

* Chairman, Task Committee on Design of FRP Bridges, Structural Engineering Committee, JSCE:
Department of Architecture and Civil Engineering, Toyohashi University of Technology,
Hibarigaoka 1-1, Tempaku-cho, Toyohashi 441-8580, Japan

In providing rational design for bridge structures, an alternative application is that of fiber reinforced polymer (FRP) composites because of their lightweight and high corrosion resistance. Also pultruded composites would be very attractive due to their continuous mass production and excellent mechanical properties. In this paper several research trials in Toyohashi University of Technology for the last decade have been introduced and some obtained dazzling results on FRP column buckling collapse tests and the fiber optic health monitoring using fiber Bragg grating sensors have been reviewed.

Key Words: Fiber Reinforced Polymer, Pultruded Shape, Local Buckling, Structural Health Monitoring

1. Introduction

In early 1980s many FRP agricultural storage silos having a lot of contents collapsed in Hokkaido (Japan) during the large axial compression or the hoop tension stresses. Then the author who engaged in Tohoku University, jointed into the working group to make the Japanese design code of the FRP silos. We have some fruits, but their contribution was very limited because new cheaper plastic bags took their role. The author moved to Toyohashi University of Technology (T.U.T.) in 1990, and in 1995 had the opportunity for studying FRP again. The fundamental experiments for the application of FRP shapes to bridges and buildings have been carried out in partnership with industries located in Toyohashi for the last decade. First, he and his co-workers confirmed the collapse behavior under tension, bending/shear and compression experimentally[1-3]. Especially the long column compression tests showed to observe periodically wavy buckles in flange plate elements at the postbuckling large deflection states[4]. Second, we dealt with the collapse of the FRP joints[5-7]. This is the one of the most important problems in the application of FRP to civil engineering structures[8]. The joint collapse has been shown to be initiated by the integral of micro-cracks in the FRP material, and these fracture behavior has been shown to be monitored through an innovative fiber optic sensing using fiber Bragg grating (FBG) sensors[9-11]. Two topics of these T.U.T. projects, the column buckling collapse and the FBG sensing for FRP joint system are reviewed in this paper.

2. Column Buckling Collapse of FRP Shapes

For the last decade, long-lived FRP materials have been used in buildings and bridges in the world; for instance, all the members of the Aberfldy Bridge[12] in Scotland, are aramid fiber reinforced polymer composite (AFRP) pedestrian bridge. It is a 113m long cable stayed pedestrian bridge, and was erected at a golf course in 1993. In Japan, carbon fiber reinforced polymer (CFRP) tubes created by a filament winding method of fabrication were adopted to the roof truss members of Mishima swimming pool[13] in 1999, and the glass fiber reinforced polymer (GFRP) beams produced by a hand lay-up method were installed to the Ikei-Tairagawa Road-Park pedestrian bridge in Okinawa in 2000[14]. On the other hand, a five-story office building[15] was constructed in Basel, Switzerland, 2000, and the columns and beams were of GFRP produced by a pultrusion fabrication method. Compared with other FRP fabrication methods, the recently developed pultrusion process is fast and suitable for large-scale production, and the products are very cheep and easily assembled to form a

structural subsystem for civil and building engineering applications. The pultrusion process is an automated assembly-line production method and is usually used to manufacture continuous lengths of FRP shapes. It has pulling devices and fiber reinforcements. These reinforcements are pulled through resin baths which saturate the fibers with thermosetting resin. Then the saturated reinforcements are then pulled through a heated die which forms the shape of the product. The products are cut into appropriate lengths by a saw.

It is well-known that in the pultruded structural members having thin-walled cross-sections local buckling occurs because of relatively low stiffness as discussed in Bank et al.[16] and Barbero and Tomblin[17]. It was suggested that for the design of a pultruded FRP structures it is very important to make an estimate of its elastic critical load, and further, it has shown how to experimentally identify mechanical properties for the estimation of buckling collapse[18-20]. In Yamada et al.[4] the identified parameters were installed in an orthotropic plate local-buckling theory and a long-column general-buckling theory.

Specimens having length L are of a pultruded 100 × 100 millimeters glass fiber reinforced polymers. The pultruded sections are composed as shown in Fig.1. The mechanical properties are listed as shown in Table 1.

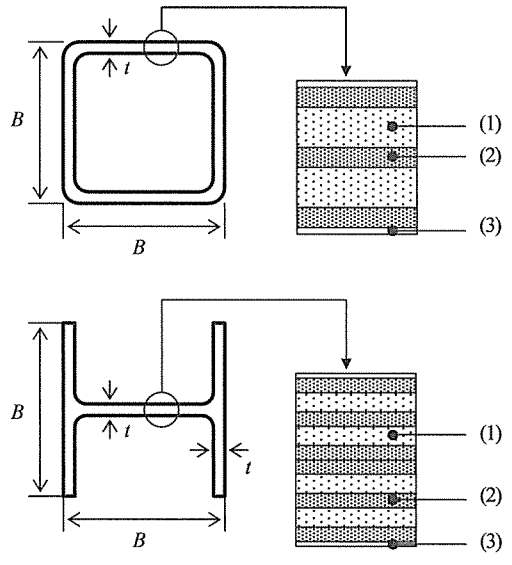

	Box-shaped	H-shaped
(1) Continuous fiber	1.725mm	1.00 mm
(2) Continuous strand mat	0.65 mm	0.65 mm
(3) Surfacing veil	0.05 mm	0.05 mm
Total thickness	5.50 mm	8.00 mm

Fig.1 Cross section

Table1 Mechanical properties of specimens

		Box-shaped	H-shaped
Young's modulus for tension in GPa	E_x	22.1	21.3
Young's modulus for bending in GPa	E_{bx} E_{by}	14.7 7.62	16.2 6.77
Poisson's ratio	ν_x ν_y	0.260 0.135	0.248 0.103
Shear modulus in GPa	G_{xy}	4.02	5.44
Compressive strength in MPa	σ_c	347	242

Let the distance between both the column support ends L_b be the present test variable. The normalized parameter for the slenderness of the specimens, λ, is defined in this study as

$$\lambda = \frac{L_b}{\sqrt{I/A}} \tag{1}$$

where I is the geometrical moment of inertia, and A the sectional area.

Figure 2 shows the schematic setup of a long column whose length is considerably larger than any of its cross-sectional dimensions. For the loading system a 2.94MN oil-pressure test machine was used. The specimen,

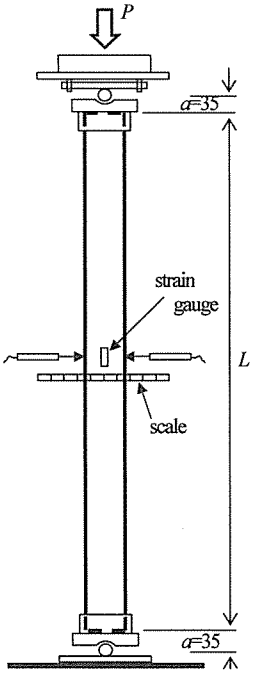

Fig.2 Long Column test

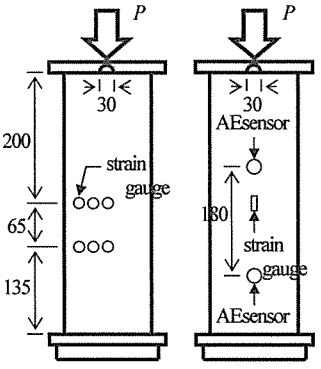

(a) Box-shaped

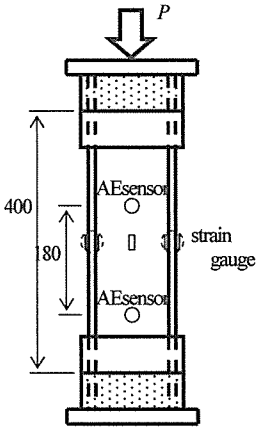

(b) H-shaped

Fig.3 Stub column test

whose ends were stiffened with steel end-jigs, was set between two steel-rod rollers in the machine, and L_b in Eq.1 are adopted to be $L+2a$. As shown in Fig.2, a is the distance from the end of specimen to the rotational center of pinned support, that is, a=35 millimeters.

A stub-column test was carried out so as to determine the local buckling load carrying capacity on the flange plate element. A box-shaped specimen having the smallest length L=400 millimeters was set in a 1.96MN oil-pressure test machine between flat-bearing steel-plates as shown in Fig.3(a). It had no pinned end, but its λ was calculated by also using Eq.1. On the other hand, at an H-shaped specimen as shown in Fig.3(b) its ends were clamped with glass fiber reinforced resin to steel jigs. Engineering strain data at the flange of the specimen were collected using a strain analyzer. Two acoustic emission sensors as shown in Fig.3 were set up and the outputs were analyzed using a commercially available system; the threshold value was 90dB, the frequency of high pass filter 100kHz, and the frequency of low pass filter 500kHz.

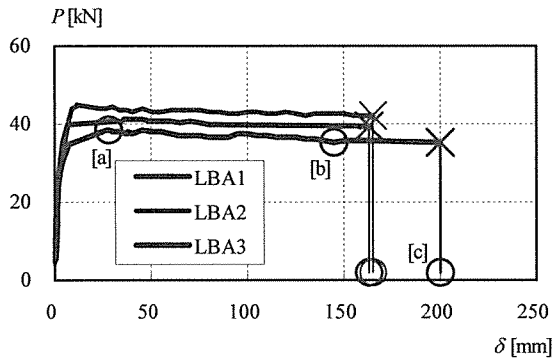

Fig.4 P–δ curves for λ=100

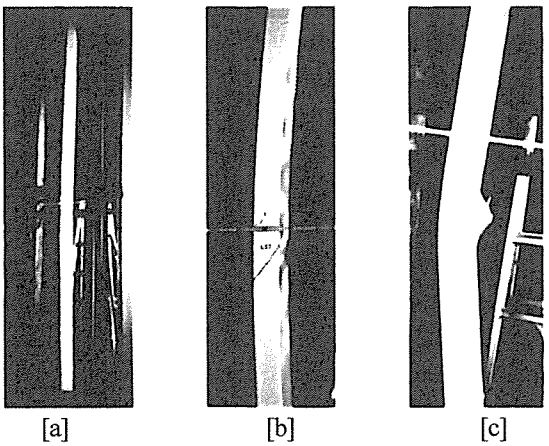

Photo 1 Various configurations for LBA3 at the equilibrium states [a], [b] and [c] associated in Fig.4

Figure 4 shows the relationships between the load and the lateral deflection at the center of the column for L=3800 millimeters (λ=100). Photo 1(a) shows to be at the state of [a] in Fig.4 for the specimen LBA3. In the photo the general (Euler type) buckling mode is observed; the mode has one-half wavelength in the longitudinal direction. Photo 1(b) depicts local buckling waves at a large deflection equilibrium state indicated with [b] in Fig.4. The rotational angle of column ($\approx 2\delta/L_b$) reached a considerably large value, say 1/13. It may be said that in these buckling tests it was discovered that it is possible to observe periodically wavy buckles from the top to the bottom; the wavelength was around 190 millimeters. At the same time, high-pitched noises, implying the micro-failure of glass-fiber or boundary-layer between the fiber and the matrix, was heard, then the collapse accompanied by loudness occurred at one part as shown in Photo 1(c). The load carrying capacity was suddenly lost almost completely.

In the case of λ=80 and 60 almost the same results as that of λ=100 have been obtained. In the case of a middle length specimen $\lambda \leq 43$, however, the collapse accompanied by loudness occurred at all the flanges at a critical load; it was much similar to the results of the stub-column tests.

The flange local buckling tests were performed so as to understand the relationship between elastic local buckling and material failure as well as to learn the ultimate compression strength of the column. Strain rosettes, which were pasted on the both outside and inside surfaces, were monitored. It was found that for the box-shaped specimens the load level at which the elastic buckling deformation develops is just prior to material failure. The bending strain components, which related to buckling mode, increase at a point above 90% of its collapse load P_{max}.

Figure 5 indicates examples of acoustic emission (AE) measurements. An acoustic emission is an elastic wave which travels through a material as the result of some sudden release of strain energy. In the figure the vertical axis is the load and the horizontal axis is the AE accumulative count. It is found that in the case of the box-shaped specimen the AE counting increases dramatically at a load level that induces elastic buckling deformation. In the case of the H-shaped specimen, on the other hand, the AE counting increases monotonously.

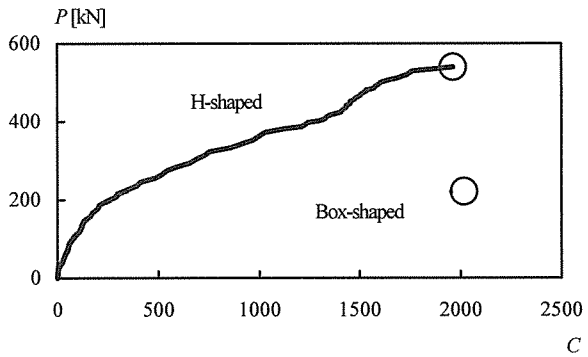

Fig.5 Load versus AE cumulative count

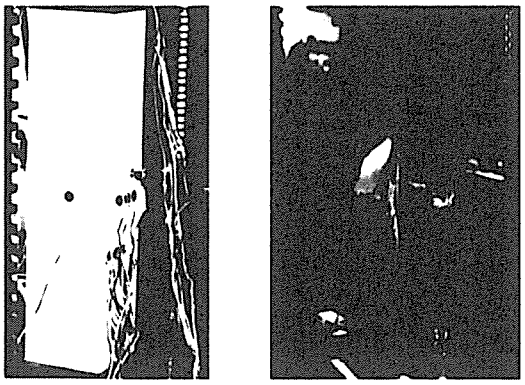

(a) Box-shaped (b) H-shaped

Photo 2 Collapse behavior

Shown in Photo 2 are that the delamination occurred in the flange of the H-shaped specimen.

For the collapse criterion of compressed stub-columns it may be useful to analyze the eigenvalue buckling problem of an orthotropic elastic plate element having thickness t. Let us consider that a supported orthotropic plate buckling due to longitudinal compression load σ to be of the mode with width B_0 and length αB_0 as inserted in Fig.6. Note that α is an unknown parameter related to the buckling wavelength and this treatment was originally proposed in Ref.1 in 1996. The fundamental membrane stress resultants, associated with axial compression load σ, are in the idealized state given by

$$n_x = -\sigma t\,,\quad n_y = 0\,,\quad n_{xy} = 0 \tag{2}$$

For the plate buckling with difference to a shell buckling problem[21], the linear membrane strain energy U_{2m} is independent of the out-of-plane deflection w as an arbitrary-small buckling mode. Consequently, the present buckling condition using a variational principal is given as

$$\delta\left(U_{2b} + V_{2m}\right) = 0 \tag{3}$$

where the first and second terms are respectively the quadratic component of the bending strain energy and the quadratic part of the interaction between the idealized prebuckling state and the nonlinear membrane stresses and strains associated with the buckling mode. These components are written as

$$U_{2b} = \frac{D}{2}\int_0^{\alpha_B B_0}\int_0^{B_0}\left[\left(\frac{\partial^2 w}{\partial x^2}\right)^2 + \frac{\nu_y}{\nu_x}\left(\frac{\partial^2 w}{\partial y^2}\right)^2 + 2\nu_y\frac{\partial^2 w}{\partial x^2}\frac{\partial^2 w}{\partial y^2} + 2\mu\left(\frac{\partial^2 w}{\partial x \partial y}\right)^2\right]dxdy \tag{4a}$$

$$V_{2m} = -\frac{\sigma t}{2}\int_0^{\alpha_B B_0}\int_0^{B_0}\left(\frac{\partial w}{\partial x}\right)^2 dxdy \tag{4b}$$

where

$$D \equiv \frac{t^3 E_{bx}}{12(1-\nu_x\nu_y)}\,,\quad \mu \equiv \frac{G_{xy}t^3}{6D} \tag{5}$$

For the flange or web of box-shaped columns, the classical simple supported boundary condition is assumed as follows,

$$w = 0\,,\ \frac{\partial^2 w}{\partial x^2} = 0 : \text{at}\ \ x = 0\,,\ \alpha_B B_0 \tag{6a}$$

$$w = 0\,,\ \frac{\partial^2 w}{\partial y^2} = 0 : \text{at}\ \ y = 0\,,\ B_0 \tag{6b}$$

where B_0=B–t. By considering satisfying this boundary condition, the buckling mode can be adopted as

$$w = w_{11}\sin\frac{\pi x}{\alpha_B B_0}\sin\frac{\pi y}{B_0} \tag{7}$$

By substituting Eqs. 7 and 4 into Eq.3 and by requiring Eq.3 to be stationary with respect to the unknown coefficient w_{11}, we can obtain the buckling load function $\sigma(\alpha_B)$. Then the minimization of $\partial\sigma(\alpha_B)/\partial\alpha_B$ leads to new expression of the critical load σ_B^{cr}.

$$\sigma_B^{cr} = \frac{\pi^2 t^2 E_{bx}}{6(1-\nu_x\nu_y)(B-t)^2}\left[\sqrt{\frac{\nu_y}{\nu_x}} + \nu_y + 2(1-\nu_x\nu_y)\frac{G_{xy}}{E_{bx}}\right] \tag{8}$$

In the case of the present box-shaped specimens, σ_B^{cr} =118 MPa for α_B=1.18 was obtained using the material properties in Table 1. Figure 7 shows the good agreement to the present experimental collapse loads dotted with open square marks. In the figure the vertical axis is the ratio of the average axial stress to the tensile strength listed in Table 1. The horizontal axis is the well-known normalized slenderness ratio.

For the web of H-shaped columns, the side edges may be changed to be clamped as

$$w = 0\,,\ \frac{\partial w}{\partial y} = 0 : \text{at}\ \ y = 0\,,\ B_0 \tag{9}$$

where B_0≡B–2t. By considering to satisfy this boundary condition, the buckling mode is adopted as

$$w = \sin\frac{\pi x}{a_w B_0}\sin\frac{\pi y}{B_0}\Sigma_i w_i \sin\frac{i\pi y}{B_0} \tag{10}$$

where i=1,3,5,7,9,11. By substituting Eqs.10 and 4 into Eq.3 and by requiring Eq.3 to be stationary with respect to the unknown coefficient w_i, we can obtain the eigenvalue equations and then the result, σ_w^{cr}=589 MPa for α_w=0.82, for the present material properties of H-shaped specimens listed in Table 1.

For the flange of H-shaped columns, the one of the side edges is changed to be free and B_0≡(B–t)/2. The buckling mode is assumed as

$$w = \sin\frac{\pi x}{a_w B_0}\Sigma_i w_i\left(\frac{y}{B_0}\right)^{i+1} \tag{11}$$

where i=1,2,3,4,5,6. By substituting Eqs. 11 and 4 into Eq.3 and by requiring Eq.3 to be stationary with respect to the unknown coefficient w_i, we can obtain the eigenvalue

equations and then the result, σ_f^{cr}=410 MPa for α_f=1.99.

Figure 7 summarizes the relationship between the present theory and experiments. The experimental collapse stresses of short box-shaped columns are approximate to σ_B^{cr}, however, the plate element criteria of H-shaped columns, σ_w^{cr} and σ_f^{cr}, are much higher than the compressive strength, σ_c. These results are in good agreement with the difference manner of the AE measurement data in Fig.5.

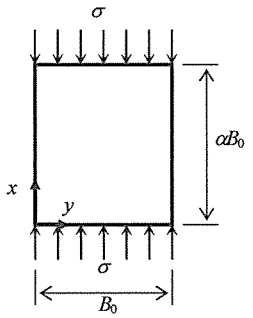

Fig.6 A plate element under compression

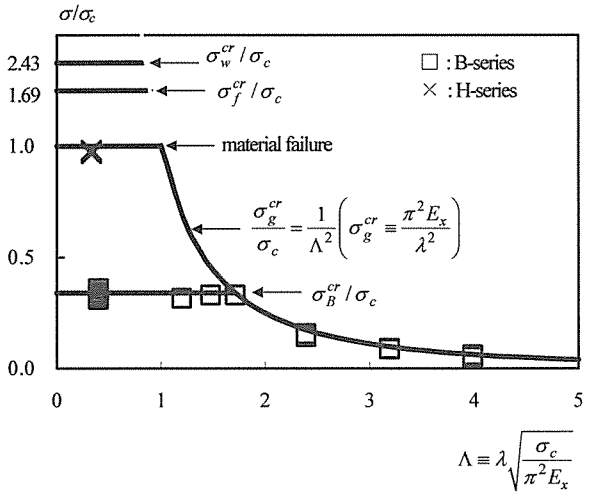

Fig.7 Relation between experiments and theory

3. Fiber Optic Sensing for the Damage of FRP Joints

FRP material is high strength, but it is relatively low stiffness. Therefore high stress concentration occurs at the joints. This means that it is necessary to reinforce the FRP member joints. For this local reinforcement, the author and co-workers[7,8] were successful in proposing to use the developed multi-axial (net fabrics) reinforcement. This local reinforcement is also suitable to the installation of new innovative fiber Bragg grating (FBG) sensors for the periodical inspection of structural health or the damage identification after earthquake disaster.

Here, the joint example of FRP members in large span roof structures using polytetrafluoroethylene (PTFE) roofing, are reviewed. For this case, it is most important to evaluate properly the structural health, and so FBG sensors were embedded in pultruded FRP members lapped over by using glass-fiber multi-axial netting polymer layers. The failure behavior of the structural FRP members connected to the PTFE membrane roofing was discussed[8,9].

Photo 3 shows the present FRP structural system, which the non-structural PTFE membrane roofing is directly connected to the flange of the structural pultruded

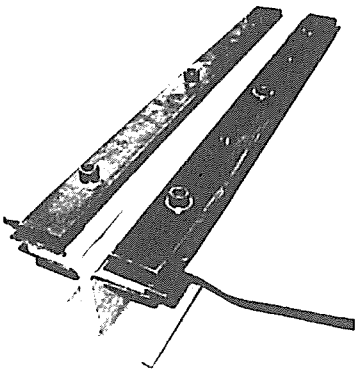

Photo 3 Detail example

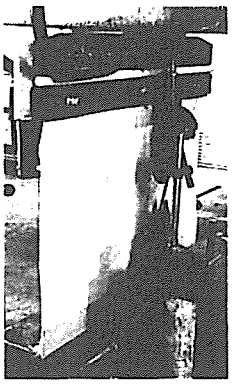

Photo 4 Test set-up

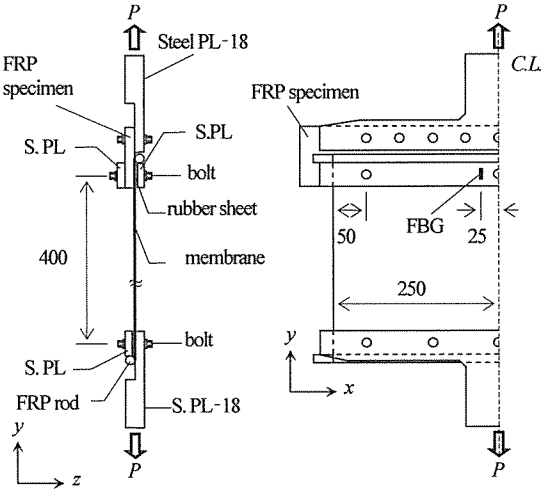

Fig.8 Dimensions of specimen

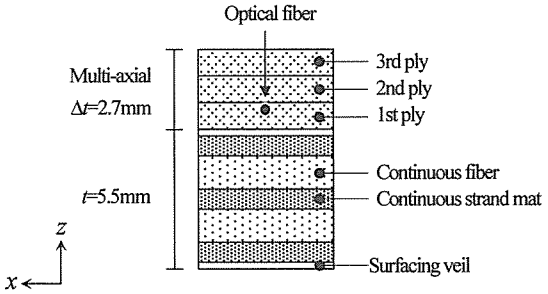

Fig.9 Cross section of the FRP member with multi-axial covering layer

FRP member. Therefore, the joint system was modeled as the flange portion as shown in Photo 4. Figure 8 shows the dimensions of the specimen; the membrane was connected to the FRP member with three M10 bolts via thin rubber sheet. The fastened torque level was here adopted to be 25N·m. In the present specimen, a pultruded glass FRP plate is of the thickness t = 5.5 millimeters and consists of two continuous fiber layers (28.3 vol%), three continuous strand mats (10.2 vol%) and two surfacing veils as shown in Fig.9.

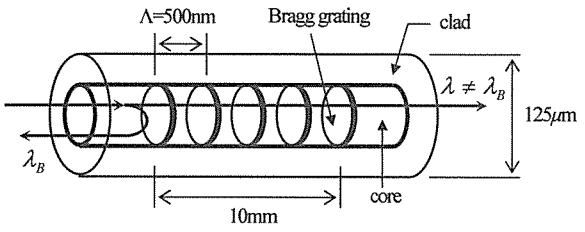

Fig.10 An optical fiber Bragg grating sensor

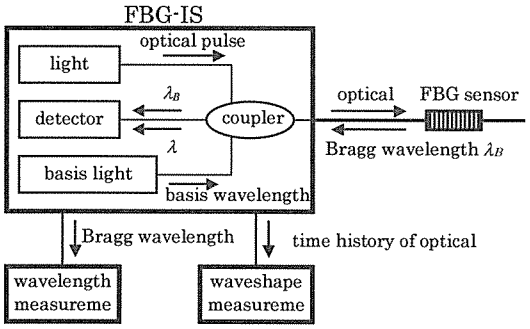

Fig.11 Diagram of measurement system

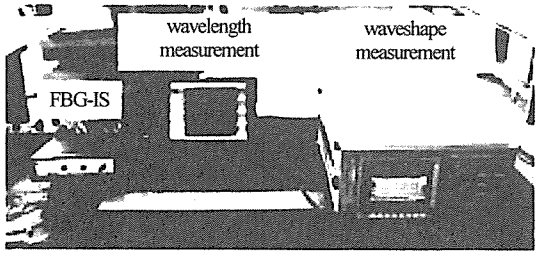

Photo 5 Measurement system

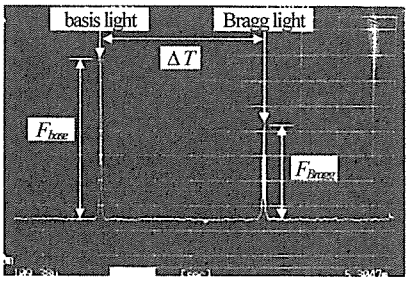

Photo 6 Time history of optical power

The strength of the structural pultruded FRP member is grater than that of the non-structural PTFE membrane roofing due to reinforcing the y-direction strength of the FRP member by using the three multi-axial layers. A fiber optic sensor was of fiber Bragg grating (FBG) here. The FBG sensor was embedded during the hand-lay-up of the second multi-axial layer and beside the center bolt as shown in Fig.8.

The fiber optic sensors in this study were adopted to be of FBG shown in Fig.10. The FBG sensor consists of the clad and the core in which the simple elements called Bragg diffraction grating are photo-imprinted[22-26]. The FBG length is 10 millimeters and the grating pitch is around 500 nanometers. Figure 11 shows the schematic diagram of the strain measurement system: the main equipment consists of the input of light with a broadband spectrum and the wavelength detection system of the narrowband component reflected by the FBG.

It is connected to the wavelength monitor and the waveshape measurement monitor as shown in Photo 5. Photo 6 shows example of waveshape measurements. As the basis light is invariable at the all times, the time difference (ΔT in Photo 6) between the peak time of the basis light and that of the Bragg light is directly related to the wavelength measurements.

Here, repeated tensile loading was performed, that is, the FRP member in the first and the second loading stage was the same, and only the PTFE membrane was changed after the first loading stage. Photo 7 shows the appearance of the FRP members beside the holes after membrane failure. In photo 7(a), no damages in the FRP members in the first loading stage were observed visually. But, in the second loading stage the damages occurred due to the bearing of bolts as referred in Photo 7(b).

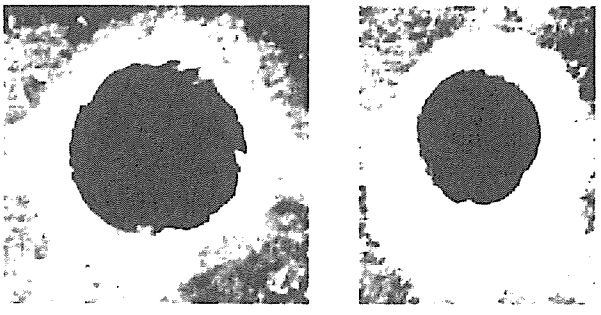

(a) After 1st loading (b) After 2nd loading

Photo 7 Appearance of the FRP members beside the holes after membrane failure

Table 2 lists the measurement data of FBG sensors at various pre-loading stages. In sensor embedding process and multi-axial laminating process, no strain was observed; and relatively large strain, which would be related to the

Table2 Results of strain measurements for pre-loading stage

specimens		initial state	after embedding	after laminating	after drilling
original data of MB303	λ_B [nm] strain ε temp. ℃	1557.272 0 [17.4]	1557.255 $-15\,\mu$ [15.9]	1557.257 $-13\,\mu$ [16.6]	1557.347 $63\,\mu$ [16.6]
revision for temperature	λ_B [nm] strain ε temp. ℃	1557.272 0 [17.4]	1557.270 $-2\,\mu$ [17.4]	1557.265 $-6\,\mu$ [17.4]	1557.355 $69\,\mu$ [17.4]

freedom of the hardening shrinkage beside the bolt hole, was obtained after drilling. But considering that the fracture elongation of FRP is over one percent-strain, normally[1], these strains are negligible in practice.

Figure 12 shows the tensile load versus the Bragg wavelength plots. Around 300 micro-strains occurred due to the effects of the fastening of bolts. In the initial loading stages the curves are approximately vertical because the friction force between the lapping surfaces would occur. After the alienation the curves have the lower slope and then bifurcate. This bifurcation behavior is shown to be related to the change of the waveshape which is defined as the shape of the equivalent optical power spectrum shown in Fig.13. Here, the vertical axis *Fop* is normalized by the optical power of the basis light. The optical power decreases as the load increases, and the shape have two peaks after reaching at a critical load. The critical load is recognized to be approximately the same as the bifurcation load in Fig.12. It would be considered that when the optical power spectrum has two peaks, the FBG becomes two different FBGs due to the occurrences of small transverse cracks inside the FRP material under locally large stress-concentration beside the bolt hole. The critical load in the first loading stage is smaller than that in second loading stage; the reason would be of the accumulation of the transverse cracks under the loading repetition. It would be possible to use these behaviors in order to estimate the structural health of the joints.

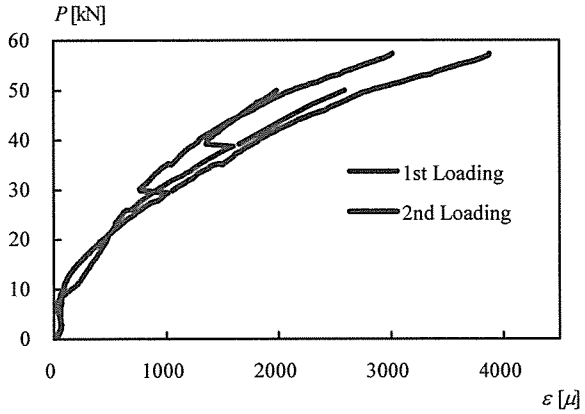

Fig.12 Load versus strain

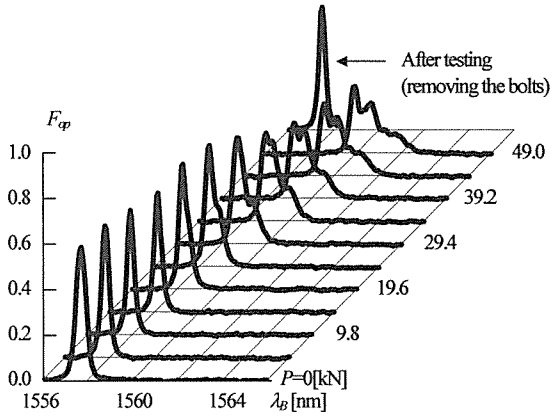

(a) MB303

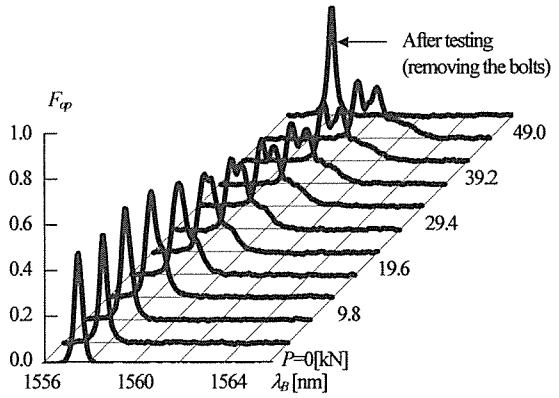

(b) MB304

Fig.13 Variations of optical power spectra

4. Conclusions

In this study, the research trials of T.U.T. Structural Laboratory supervised by the author have been reviewed. Suggested are that in FRP shapes the buckling problem of plate elements and the micro-damage at the joints are very important and have to be more encouraged to study for the development of FRP application to bridge construction in the future.

References

1) Yamada S. and Komiya I., Elastic deflection behavior of a box-shaped pultruded composite member and its collapse, Fiber Composites in Infrastructure, ICCI'96,

pp. 699-707, 1996
2) Yamada, S., Takashima, H., Tadaka, R. and Komiya, I.: Experiments on the buckling and collapse of pultruded composite columns under axial compression, Fiber Composites in Infrastructure, ICCI'98, Vol.2, pp.236-247, 1998
3) Yamada, S., Komiya, I. and Nakazawa, H.Y.: Collapse of box-shaped pultruded fiber reinforced polymeric matrix composites under compression, J. Struct. Constr. Eng., AIJ, No.518, pp.49-56, 1999. (in Japanese)
4) Yamada, S., Nakazawa, H.Y. and Komiya, I., Buckling and collapse of pultruded fiber reinforced polymer member under compression, APCS Symp., SEOUL, Vol.2, pp.961-968, 2000
5) Yamada S., Nakazawa H.Y., Fukatsu N., and Komiya I., Experiments on the connection collapse of pultruded fiber reinforced polymeric composites, CD-ROM Proc. IASS Symp., TP071, 2001
6) Yamada, S., Nakazawa, H.Y. and Komiya, I.: Fiber optic sensing of the joints of fiber reinforced polymer structures, CD-ROM Proceedings, Structural Engineers World Congress, No.T3-1-a-2, 2002
7) Nakazawa, H.Y. and Yamada, S.: Health monitoring using FBG sensors for structural members, Proceedings International Workshop on Structural Health Monitoring of Bridges, JSCE, pp.121-126, 2003
8) Yamada, S., Nakazawa, H.Y. and Komiya, I.: Hearth monitoring of long-lived structural members reinforced with fiber multi-axial netting polymer layers having fiber optic sensors, Advancement of Material and Processing Engineering, SAMPE, pp.183-186, 2003
9) Yamada, S., Nakazawa, H.Y., Matsumoto, Y. and Komiya, I.: Fiber Bragg grating sensing for long-lived fiber reinforced polymer structures, CD-ROM Proceedings of International Association for Bridge and Structural Engineering Symposium, IABSE, 3S, SHA220, pp.1-6, 2004
10)Nakazawa, H.Y., Yamada, S. and Komiya, I.: Collapse of structural FRP members connected to PTFE membrane roofing and the health monitoring using optical fiber sensors, CD-ROM Proceedings of IASS-APCS2003, 2003
11)Yamada, S.: Fiber optic sensing for the structural health of long-lived building and bridges, Proceedings of the International Workshop on Sustainable Urban and Building Design, Toyohashi University of Technology, pp.123-131, 2003
12)Harvey, W.J.: A reinforced plastic footbridge, Aberfeldy, UK, Structural Engineering International, IABSE, pp.229-232, 1993
13)Fukuyama, H.: FRP composites in Japan, Concrete International, Oct., 1999
14)http://www.pwrc.or.jp/kaihatsu/kaihatsu14.html
15)Keller, T.: Towards structural forms for composite fibre materials, Structural Engineering International, Vol.9, No.4, pp.297-300, 1999
16)Bank, L.C., Gentry, T.R. and Nadipelli, M.: Local buckling of pultruded FRP beams analysis and design, 49th Annual Conference, SPI, 1994
17)Barbero, E. and Tomblin, J.: A phenomenological design equation for FRP columns with interaction between local and global buckling, Thin-Walled Structures, Vol.18, pp.117-131, 1994
18)Blosser, R., Florio, J. and Donti, P.: Continuous resin transfer molding of high quality, low cost, constant cross section, composite structural elements, 39th Int. SAMPE Symp., pp.1961-1972, 1994
19)Tomblin, J. and Barbero, E.: Local buckling experiments on FRP columns, Thin-Walled Structures, Vol.18, pp.97-116, 1994
20)Vinson, J.R. and Sierakowski, R.L.: The Behavior of Structures Composed of Composite Material, Mantinus Nijhoff Publishers, 1986
21)Yamada, S. and Croll, J.G.A.: Contributions to understanding the behavior of axially compressed cylinders, Journal of Applied Mechanics, ASME, Vol.66, pp.299-309, 1999
22)Kersey, A.D., et al.: Progress towards the development of practical fiber Bragg grating instrumentation systems, SPIE, Vol.2829, 1996
23)Okabe, Y., Tsuji, R. and Takeda, N.: Measurement of transverse thermal residual strain in CFRP laminates using FBG sensors, Advancement of Material and Processing Engineering, SAMPE, pp.171-174, 2003
24)Yamada, S.: Fiber Bragg grating sensing for the plastic failure of steel dampers in passive control system, Proceedings of International Symposium on Earthquake Engineering, 2005
25)Yamada, S., Matsumoto, Y., Yagi, S. and Taguchi, T.: Cyclic tests of vibration control system in steel buildings and its fiber optic sensing, Proceedings of AESE, pp.633-640, 2005
26)Yamada, S., Matsumoto, Y., Hiramoto, T. and Yamada Satoshi: Fiber optic sensing for steel bridges, Proceedings of AESE, pp.627-632, 2005